IEEE Access
Multidisciplinary | Rapid Review | Open Access Journal

Received June 28, 2020, accepted July 2, 2020, date of publication July 13, 2020, date of current version July 22, 2020.

Digital Object Identifier 10.1109/ACCESS.2020.3008551

Back-to-Back Microstrip Antenna Design for Broadband Wide-Angle RF Energy Harvesting and Dedicated Wireless Power Transfer

PEI ZHANG[1], HAO YI[1], HAIXIA LIU[1], (Member, IEEE), HONG YANG[2], GUOFEI ZHOU[2], AND LONG LI[1], (Senior Member, IEEE)

[1]Key Laboratory of High Speed Circuit Design and EMC of Ministry of Education, Collaborative Innovation Center of Information Sensing and Understanding, School of Electronic Engineering, Xidian University, Xi'an 710071, China
[2]First Research Institute of Ministry of Public Security of PRC, Beijing 100044, China

Corresponding author: Long Li (lilong@mail.xidian.edu.cn)

This work was supported by the National Key Research and Development Program of China.

ABSTRACT A novel back-to-back microstrip antenna is proposed to cover 2G/3G/4G/5G communication bands and ISM-2.4 GHz, ISM-5.8 GHz to simultaneously realize broadband wide-angle ambient wireless energy harvesting and dedicated wireless power transfer. The ground mode radiation is introduced by the limited-sized ground, with the loading of the patches and shorting vias, to form a broadband resonance from 2 GHz to 4 GHz. Furthermore, a resonance at ISM-5.8GHz is also excited with high-directivity. On the basis of ensuring miniaturization (e.g. $0.28\lambda_0 \times 0.22\lambda_0 \times 0.05\lambda_0$ for 2 GHz) and compactness, omnidirectional radiation in broadband resonance and bi-directional radiation at 5.8 GHz are realized by the 'back-to-back' combination of two antenna elements. Measured results show that an over 67.2% impedance bandwidth (2.03 GHz∼4.08 GHz) is obtained. Through the wireless power transmitting and receiving test, the angular stability of above ±60° for wireless energy harvesting is achieved at the mainstream operating frequencies. At ISM-2.4 GHz RF power of up to -8.5 dBm can be harvested at a distance of 0.5 m from the transmitter with the transmitting power of 12.5 dBm, while it is -8.9 dBm at ISM-5.8 GHz, which validates the effectiveness for WEH/WPT.

INDEX TERMS Wireless power transfer, wireless energy harvesting, broadband, wide-angle, miniaturization.

I. INTRODUCTION

Recently there has been an upsurge of research interests in wireless sensor network (WSN) with the rapid development of internet of things (IoT) [1]. It is worth noting that in the future, billions of wireless sensors will be powered by which kind of energy [2]. Energy autonomous or batteryless will become an inevitable trend. Possible solutions include ambient wireless energy harvesting (WEH) [3] and periodic charging through wireless power transfer (WPT) [4], [5].

Ambient radio frequency(RF) energy harvesting [6] is becoming a powerful alternative due to its advantages of passive, all-weather and all-round. The current ambient RF energy is mainly distributed in the communication band and WiFi band from hundreds of megahertz to 3 GHz (such as 2G-GSM, 3G-UTMS, ISM-WiFi-2.4 GHz and 4G-LTE). In addition, with the gradual popularization of 5G technology, the 5G-IMT band operating at around 3500 MHz is also a power source that cannot be ignored. Therefore, one of the major concerns in designing the receiving antenna is the characteristic of broadband or multi-band. Several kinds of dual-band or tri-band antenna or rectenna are proposed to realize WEH at GSM-band and UTMS-band [7]–[10]. A novel six-band dual circular polarization rectenna for WEH is presented [11] with a wide bandwidth (from 550 MHz to 2.5 GHz) and a compact size. While for broadband, reference [12] presents a novel broadband cross-dipole antenna with flower-shaped slot to realize better impedance matching from 1.8 GHz to 2.5 GHz. Reference [13] proposed a compact and broadband slotted antenna which performs well at LTE band with a wide bandwidth from 2 GHz to 3.1 GHz. However, due to the scattered distribution of communication band and ISM band,

The associate editor coordinating the review of this manuscript and approving it for publication was Waleed Ejaz.

it is difficult to cover more frequency points solely by broadband, either the bandwidth range of the multi-band antenna is difficult to cover all channels of the communication bands.

On the other hand, the receiving antenna of WEH terminals need to maintain wide-angle and multi-polarization characteristics as much as possible. The introduction of metasurface [14]–[19] provides a solution to the issue. To extend the narrow beam of the conventional high-gain rectenna, the multiport and multi-beam antenna is promising. The harvesting angle range is extended by combining two tilted beams and can be greater than 70° [20]. Multiport is also becoming a focus of WEH terminal antenna design [21]. The advantages of the multiport pixel approach include enhanced harvested RF power for a given area as well as a reduction in the antenna matching requirements.

However, the magnitude of ambient RF power is too low, around $-40\sim-50$ dBm [22]. Therefore, when the power obtained by WEH cannot meet the power demand of the sensor, an active power supplement scheme is needed. One method is to harvest the hybrid ambient energy such as solar energy, kinetic energy, and thermal energy, etc [23]–[26]. The other one is to combine the active WPT for charging. The main challenge of the former is whether the hybrid energy sources can meet the power demand of sensors in all-weather and all-round conditions, and how to realize miniaturization and integration of the hybrid energy harvesting devices. In contrast, the solution combining active WPT charging is completely based on the RF power, thus the structure is simple, and the power level is guaranteed. But for now, few articles focus on the design of the antenna for simultaneous WEH and WPT. For WEH antenna, it is desirable to have broadband or multi-band characteristics, and the radiation pattern is preferably omnidirectional due to the ambient electromagnetic waves (such as transmitted from outdoor communication base station or indoor WiFi router) comes from different directions. At the same time, WPT works under active conditions at a certain operating frequency and towards a certain direction, which requires high directional radiation pattern. Sometimes, bi-directional radiation could show more advantages than single-directional radiation. In the power supply issue of wireless sensor network, we often face the scene that a large number of sensors are distributed in a region, which is a static state. While the power sources are in a dynamic state, which are moving and rotating in a certain path, thus spreading the beam in all directions to realize the power supply for each sensor. At this point, the advantage of bi-directional radiation becomes apparent, meaning that wireless power can be obtained from two completely opposite directions, which helps simplify route planning and charging costs for the power source.

The wideband omnidirectional characteristic of antenna is not difficult to realize based on antenna structures such as monopole. However, how to make ambient WEH antenna and directional WPT antenna work simultaneously and integrate on a miniaturized terminal to charge wireless sensors is undoubtedly challenging and of significant practical value.

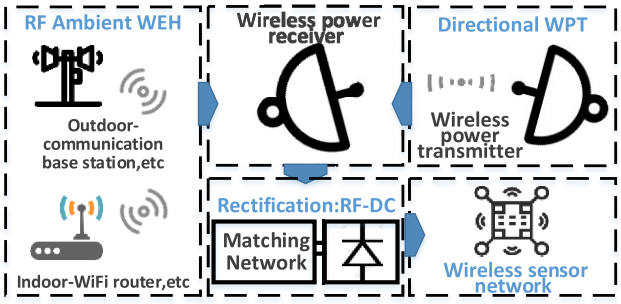

FIGURE 1. Framework of simultaneous RF ambient WEH and directional WPT for power supply of wireless sensor network.

Fig.1 illustrates the framework of wireless sensors power supply solution by simultaneous WEH and WPT.

Based on the above concerns, a novel back-to-back microstrip antenna is proposed to cover 2G/3G/4G/5G communication bands and ISM-2.4 GHz, ISM-5.8 GHz to simultaneously realize broadband wide-angle ambient WEH and directional WPT. Section II described the design and simulation of the proposed antenna. The radiation performance of the proposed antenna is given in Section III. Section IV illustrates the wireless power transmitting and receiving test and the analysis of the measured results to validate the practicality and reliability of the proposed antenna for WEH/WPT.

II. ANTENNA DESIGN AND SIMULATION

A. ANTENNA GEOMETRY

The proposed antenna is composed of two identical microstrip antenna elements [27], which are respectively named Face A and Face B. Fig.2 illustrates the overall geometry of the proposed antenna element, which consists of one layer of metal patches, two layers of dielectric substrates and an aperture-coupled feeding structure. As shown in Fig.2(a), a driven patch is set at the center above the upper-layer substrate, which is with the size of $L_{patch} \times W_{patch}$. A pair of symmetrically arranged parasitic patches are positioned on both sides of the driven patch. The size of the parasitic patches is $L_{para} \times W_{para}$. The driven patch and the parasitic patches have the same width to facilitate the conformality of the antenna element, but there is an adjustment degree of freedom in length. The spacing between the driven patch and the parasitic patch is g_x. The ground plane is printed on the bottom of the upper-layer substrate, where the coupled slot is etched with the size of $L_{slot} \times W_{slot}$. The size of the ground plane is small, which is the same as that of the radiator composed of the driven patch and the parasitic patches. The total size of the antenna element is $L_{sub} \times W_{sub}$. The parasitic patch pairs are respectively provided with a set of symmetrically arranged shorting vias, each set of 4. The spacing between two sets of the shorting vias is S_1, while the spacing of the adjacent shorting vias is S_2, and the via radius is r. It is a three-layer structure where the upper and the lower dielectric substrates are made of F4B, which is with the relative permittivity of 2.65, loss tangent of 0.002, and thickness of h_1 (the upper-layer) and h_2 (the lower-layer).

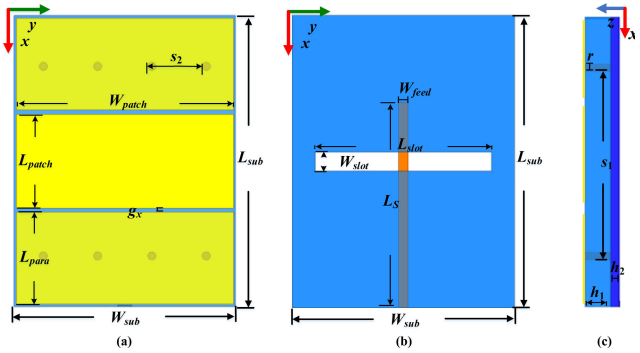

FIGURE 2. Geometry of the proposed antenna element: (a) Top view of the top layer structure; (b) Top view of aperture-coupled feeding structure; (c) Side view of the overall structure.

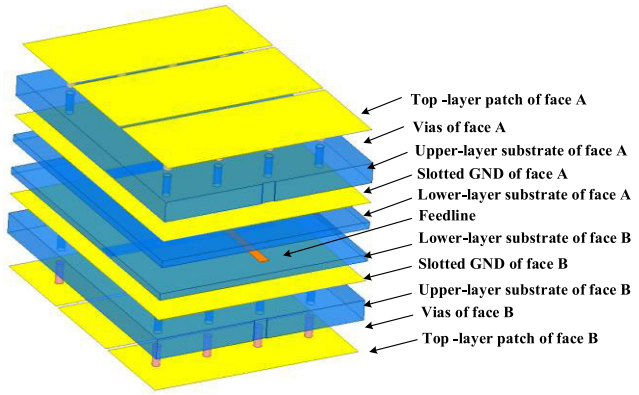

FIGURE 3. Perspective view of the geometry of the proposed back-to-back antenna.

The antenna element is center-fed by the microstrip slot-coupling structure. The 50 Ω microstrip line is printed on the bottom-layer of the lower substrate, whose length and width is L_S and W_{feed}. It should be noted that we make the substrate size slightly larger than the ground plane size by 0.6 mm in each direction in order to ensure more accurate PCB processing.

The two elements are combined by the form of 'back-to-back', which means Face A and Face B's lower-layer dielectric substrate fits completely and shares the feedline. The specific combination is shown in Fig.3, which depicts the perspective view of the geometry of the proposed back-to-back antenna. It is worth noting that in 'back-to-back' combination, the microstrip feeding line is replaced by a strip line, whose characteristic impedance is about half that of the microstrip line. Thereby, to match the 'back-to-back' antenna to 50 Ohm, the input impedance of the single patch antenna is about 100 Ohm.

B. OPERATING MODES ANALYSIS

The full-wave simulation is performed using the High Frequency Structure Simulator (HFSS) and the optimized parameters are shown in Table 1. Fig.4 presents the simulated reflection coefficients of the antenna. As shown in Fig.4, the proposed antenna forms resonances at approximately the following three frequencies: 2.1 GHz, 3.5 GHz and 5.8 GHz.

TABLE 1. Dimensions of the designed antenna.

Parameter	Description	Value (mm)
L_{sub}	Length of the substrate (both of the upper-layer and the lower-layer)	42.6
W_{sub}	Width of the substrate (both of the upper-layer and the lower-layer)	32.6
L_{patch}	Length of the driven patch	13.8
W_{patch}	Width of the driven patch	32
L_{para}	Length of the parasitic patch	13.5
W_{para}	Width of the parasitic patch	32
L_s	Length of the feedline	30
W_{feed}	Width of the feedline	1.4
L_{slot}	Length of the slot	25.9
W_{slot}	Width of the slot	2.8
g_x	Spacing between the driven patch and the parasitic patch	0.6
s_1	Spacing between two sets of the shorting vias	27.3
s_2	Spacing of the adjacent shorting vias	8
r	Radius of the via	0.6
h_1	Thickness of the upper-layer substrate	3
h_2	Thickness of the lower-layer substrate	1

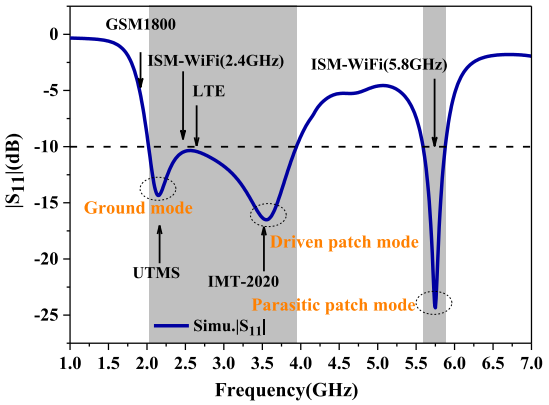

FIGURE 4. Simulated reflection coefficients of the proposed antenna.

The broadband radiation mechanism of the proposed antenna element is elaborated in [27]. In short, by introducing a limited-sized ground plane to participate in radiation, the 'ground mode' is formed corresponding to the resonance at 2.1 GHz; The original 'driven patch mode' of microstrip patch antenna is at 3.5 GHz. It is worth mentioning that the 'driven patch mode' resonance should appear at around 4.8 GHz, which means the two resonant modes are separated from each other. It cannot meet the demand of covering the most channels of the communication bands. Here, the loading of the driven patch and the pair of parasitic patches play an important role, moving the resonance point from 4.8 GHz to lower frequency but hardly change the resonant mode around 2.1 GHz. The loading of the shorting vias further moves the 'slot mode' to lower frequency, while improving the impedance matching of the antenna, eventually forming a broadband resonance from 2.02 GHz to 3.94 GHz. It covers the communication bands including 2G-GSM1800, 3G-UTMS, ISM-WiFi, 4G-LTE and 5G-LMT, which makes it possible to harvest the ambient RF energy of each channel in the above communication bands.

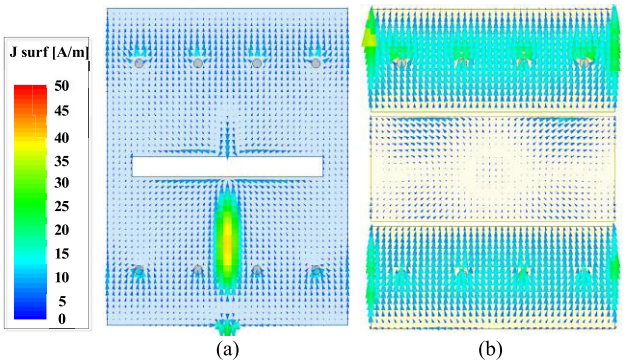

FIGURE 5. Simulated current distribution of (a) the ground plane and (b) the top-layer patches at 5.8 GHz.

At the same time, the high-degree-of-freedom design of parasitic patch loading and shorting via loading can excite the resonant mode around 5.8 GHz, which is corresponding to another ISM-WiFi band. The simulated current distributions of the ground plane and top-layer patches at 5.8 GHz are shown in Fig.5. As can be seen in Fig.5, the slot coupled RF power from ground to the top-layer patches, while the driven patch coupled the RF power to the parasitic patches at both sides. The current on parasitic patches is evenly distributed and in the same direction, and the radiation is mainly carried out through the two edges of the patch. The radiation patterns of parasitic patches at both sides are superimposed on each other in the same direction, thus forming a good radiation directivity at 5.8 GHz.

C. OMNIDIRECTIONAL APPROACH (BACK-TO-BACK COMBINATION)

For the broadband resonance (hereinafter referred to as band A) of the single antenna element, the H-plane pattern is omnidirectional, while the E-plane pattern is kind of like a dipole along the x-direction. Although the beamwidth is relatively wide, there are nulls at both ends, which means some certain blind zones exists in the direction of both ends in ambient WEH. Additionally, low-frequency region shows better omnidirectivity. As the frequency increases, the directivity of E-plane pattern is getting stronger. In order to further expand its omnidirectivity, Face A and Face B are combined in a back-to-back to share the feedline, so that the E-plane of both the antenna elements connect with each other, while the H-plane patterns keep the omnidirectivity.

For the other resonance around 5.8 GHz (hereinafter referred to as band B), the in-phase superposition at 5.8 GHz produces a narrow beam, which means the pattern has better directivity. As the consequence, with a miniaturized and compact structure, the electromagnetic waves from all directions in the free space can be harvested as much as possible. Fig.6 shows the simulated three-dimensional patterns and the maximum gain at the main operating frequencies. In band A, the patterns show good omnidirectivity, while Band B exhibits bi-directional radiation with strong directivity, that

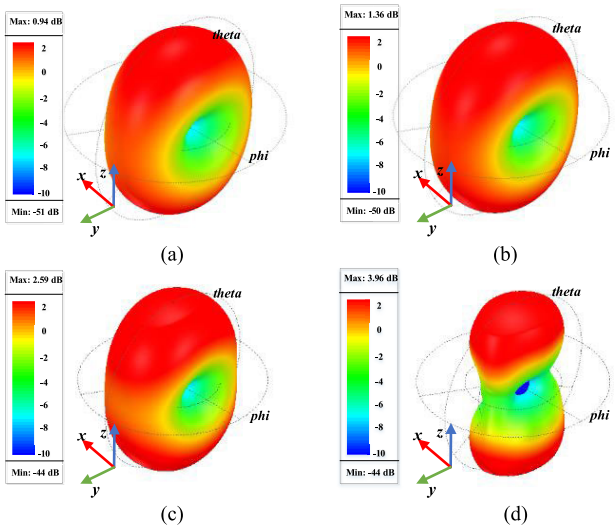

FIGURE 6. Simulated three-dimensional radiation patterns and the maximum gain at: (a) 2.1 GHz; (b) 2.4 GHz; (c) 3.6 GHz; (d) 5.8 GHz.

is, each antenna element exhibits good broadside radiation characteristics. The maximum gain is about 3.96 dBi.

III. ANTENNA PERFORMANCE MEASUREMENTS

In order to validate the preceding simulation of the proposed back-to-back microstrip antenna, the prototype with the same parameters as discussed in Section II was fabricated. The overall size of the proposed antenna is 42.6 mm$\times$32.6 mm$\times$8 mm ($0.28\lambda_0\times0.22\lambda_0\times0.05\lambda_0$ for 2 GHz). In order to facilitate the processing, the two antenna elements are processed separately. The feedline is connected with the inner conductor of the SMA connector by welding and to keep the bottom layer glued flat. The ground planes of Face A and Face B are led out respectively to weld the outer conductor of the SMA connector. Therefore, impedance matching and the symmetric feeding can be obtained.

However, it shall be noted that the antenna structure introduces the 'ground mode'. Due to the omnidirectional pattern, induced current is caused, thus the outer conductor of SMA connector is connected to the cable when it is under the test situation. It will cause the extension of the size of the ground plane, leading to the problem of ripple of the pattern and the deterioration of the resonance characteristics. In order to solve this problem, a ferrite magnetic ring is placed at the connection between the antenna port and the cable to isolate the current of the outer conductor, thereby to alleviate the deterioration caused by the extension of ground plane size.

The reflection coefficient of the proposed antenna is measured with a vector network analyzer (VNA) of Agilent N9918A. The prototype and the measured reflection coefficient are depicted in Fig.7. It is not difficult to find that the measured reflection coefficient is basically consistent with the simulation results. For band A, a 67.2% -10 dB impedance bandwidth from 2.03 GHz to 4.08 GHz is achieved, which is good enough to cover the communication bands previously mentioned. For band B, the resonance is

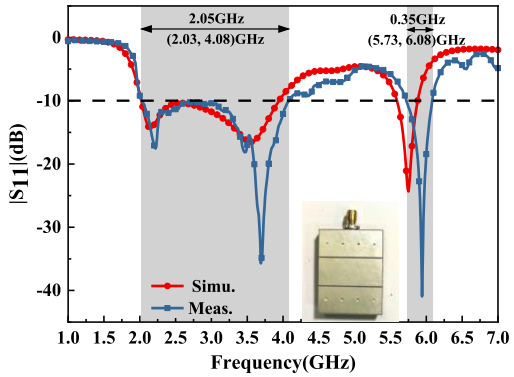

FIGURE 7. Prototype, the simulated and measured reflection coefficient of the proposed antenna.

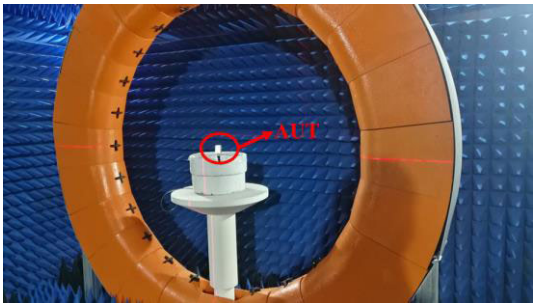

FIGURE 8. Actual scenario of antenna erection on the multi-probe platform in the microwave anechoic chamber.

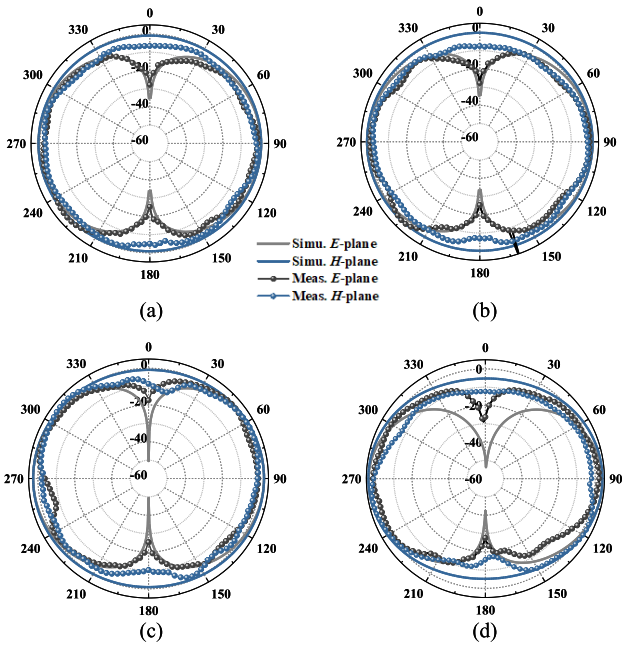

FIGURE 9. Measured and simulated radiation patterns at (a)2.2 GHz; (b)2.4 GHz; (c)3.6 GHz; (d)5.8 GHz.

at 5.9 GHz, with a frequency offset of 100 MHz comparing to the simulated result. The actual bandwidth of band B is 350 MHz, which could meet the demand of directional WPT at 5.8 GHz. To sum up, the broadband characteristic of the proposed antenna is well verified. The radiation patterns are measured on the multi-probe test platform in the microwave anechoic chamber. The actual antenna test environment is shown in Fig.8. The measured patterns at respectively 2.2 GHz, 2.4 GHz, 3.6 GHz and 5.8 GHz are shown in Fig.9. The measured boresight gains and the measured antenna total efficiency at main operating frequency bands are listed in the table 2.

TABLE 2. Realized Boresight gain and total efficiency of the proposed antenna.

	2.2 GHz	2.4 GHz	3.6 GHz	5.8 GHz
Simu-Gain/dB	0.94	1.36	2.59	3.96
Meas-Gain/dB	-0.42	0.19	0.91	2.40
Total-Efficiency	77.5%	82.5%	71.4%	69.9%

It can be observed from Fig.9 that the measured and simulated patterns show good consistency at 2.2 GHz and 2.4 GHz. At 3.6 GHz and 5.8 GHz, the H-plane and E-plane patterns has a certain difference around direction $\theta = 0°$ and the direction $\theta = 180°$, and in some directions, the patterns have some defects. Compared with the simulated results, the measured boresight gain is generally 1-1.5 dB smaller. The measured antenna efficiency is within the range of approximately 70%-85%. But in general, the measured patterns basically satisfy the requirements of omnidirectional WEH and dedicated WPT. The problems above could be attributed to two parts: 1) The use of ferrite magnetic ring has alleviated the problem of the extension of ground plane size to a certain extent, but it has not been completely solved; 2) In order to simplify the processing difficulty, the two antenna elements are separately processed and then bonded, and the error caused by the manual operation causes the impact on the radiation performance of the antenna. This problem should be better solved after improving the processing method.

IV. WEH PERFORMANCE

In order to analyze the WEH performance of the proposed antenna, a dual-port full-wave simulation model is built in HFSS. The horn antenna is port-1 as a RF source to simulate free-space incident waves in the actual environment. The proposed back-to-back antenna is set as port-2 as a wireless energy harvesting antenna, and is placed at a distance of 0.5 m away from the horn to ensure that it is in the far-field region of the transmitter.

Set the transmitting power of the horn is 1W, the power harvesting efficiency η of the receiving antenna can be obtained from the ratio of p_r and p_{sum}, where p_r is the total power harvested by the receiving antenna, and p_{sum} presents the power distributed over the aperture of the receiving antenna in space. The specific formula is as follows:

$$\eta = \frac{p_r}{p_{sum}} = \frac{mag(|S_{21}|)^2}{\iint\limits_s \vec{E} \times \vec{H} \cdot dS} \tag{1}$$

where p_r could be derived from the S-parameters in full-wave simulations; while p_{sum} could be obtained by Poynting vector integration of the E-field distribution on the spatial aperture of the receiving antenna. Keeping the position of the proposed

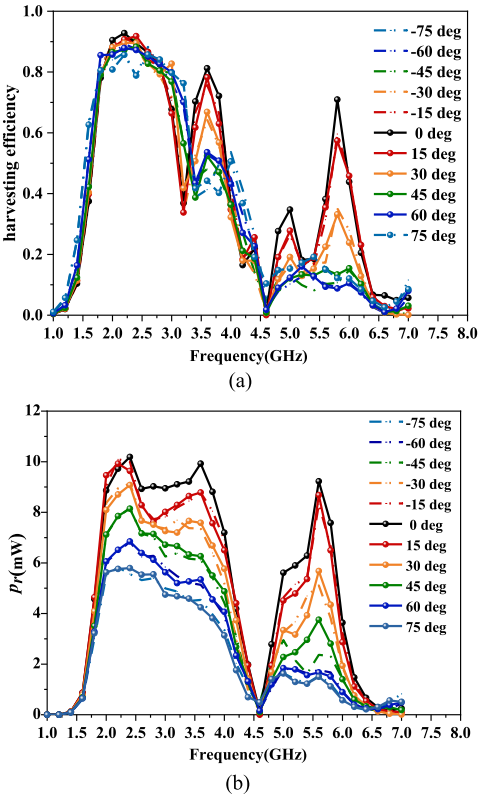

FIGURE 10. WEH performance of the proposed antenna as a function of frequency and rotation angle: (a) WEH efficiency; (b) harvested power.

antenna fixed, which means maintaining the distance from the proposed antenna unchanged and polarization alignment, let the horn rotate by ±15°, ±30°, ±45°, ±60° and ±75° respectively. By simulating the incoming waves from all directions in the actual environment, WEH angular stability of the proposed antenna could be achieved. The harvested power by the antenna and the harvesting efficiency are shown in Fig.10. It can be observed that when the receiving antenna is located in the maximum radiation direction of the horn, that is, the horn rotation angle is 0°, the harvested power and the harvesting efficiency can basically reach a maximum value. The maximum harvested power of 10.2 mW can be obtained at 2.4 GHz, corresponding to the harvesting efficiency of 90%. The maximum harvested power of 9.9 mW can be obtained at 3.6 GHz, while the harvesting efficiency reaches 81%. The maximum harvested power of 9.2 mW can be obtained at 5.8 GHz, and the harvesting efficiency is 70%. It is worth noting that RF power above 8 mW can be achieved from 2 GHz to 4 GHz and at 5.8 GHz, and the harvesting efficiency at the main operating frequency is basically greater than 80%. It illustrates that the proposed antenna can achieve high-efficiency broadband and multi-frequency WEH of ambient RF power.

In terms of WEH angular stability, as seen in Fig.10, from 1.8 GHz to 3 GHz (covering 2G-GSM1800, 3G-UTMS, ISM-WiFi and 4G-LTE), harvesting efficiency of 80% in the range of ±75° can be obtained. The 5G-IMT band around 3.6 GHz

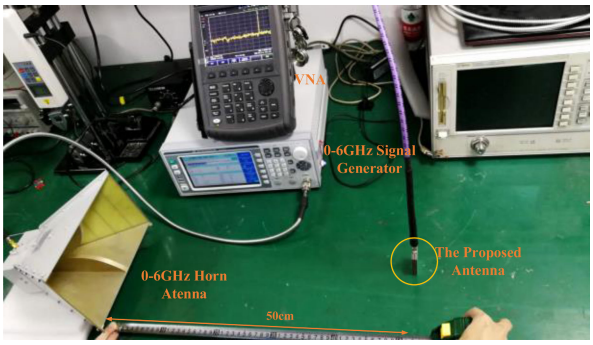

FIGURE 11. Wireless power transmitting and receiving system test system for verification of the WEH and WPT performance of the proposed antenna.

can achieve nearly 70% harvesting efficiency within ±30°, while the 5.8 GHz ISM band can achieve more than 60% harvesting efficiency within ±15°. In band A from 2 GHz to 4 GHz, the harvested power of above 5 mW could be achieved within ±60°, while in band B around 5.8 GHz it is within ±30°. Therefore, the WEH full-wave simulation results can be matched with the antenna pattern characteristics previously analyzed. In band A, the radiation of the proposed antenna is more omnidirectional and is suitable for omnidirectional harvesting of ambient RF power. As the frequency increases, the directivity of the antenna gradually increases. In practical applications, 5.8 GHz can be used as a power transmitting and receiving band for directional WPT without disturbing the normal operation and energy harvesting of the communication band.

The actual test platform was built to verify the WEH performance of the proposed antenna. The DC-6 GHz signal generator is used as the RF power source, and is radiated from the 0.5 GHz-6 GHz horn antenna. The use of a foam board to properly raise the horn antenna facilitates reducing the reflection and scattering effects of the surface of the test platform. The receiving antenna is placed 50 cm away from the port surface of the horn, and connected to the Agilent vector network analyzer (VNA) as a wireless spectrum power meter, which can directly obtain the data display of the harvested power. The diagram of the actual test system is shown in Fig.11.

The default transmitting power of the HFSS software in the full-wave simulation is 30 dBm (1W), and the maximum received power is 10 dBm (10 mW), which means the loss is 20 dB. The maximum RF power generated by the signal generator is 15dBm. The insertion loss of the transmitting cable and the receiving cable is measured at 1 GHz-6 GHz and the sum is around 2.5 dB. Therefore, considering the cable insertion loss, the ideal harvested power should be about −7.5 dBm. The curves of harvested power in the actual test at each operating frequency are presented in Fig.12. The maximum harvested power of the proposed antenna at 2.4 GHz is −8.5 dBm, which is about 1 dB less than the ideal result, which is about 0.03 mW. It may be due to the relatively complex electromagnetic environment of the test platform, which

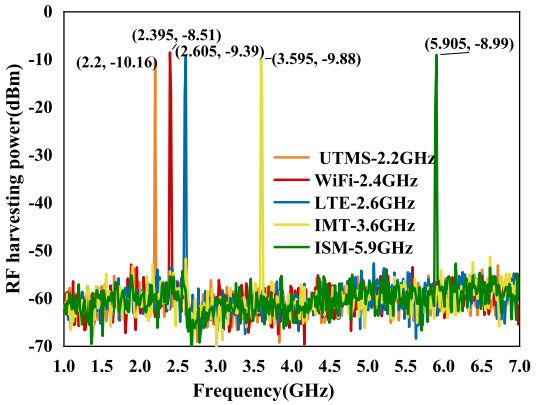

FIGURE 12. Harvested RF power by the proposed antenna in the test system at each operating frequency.

is within the acceptable error range. It also proves the WEH performance of the proposed antenna. The maximum harvested power is kept at around −10 dBm within the rotation range of ±60° with constant polarization alignment, which proves that the antenna has good WEH angular stability. The other operating frequencies such as 3G-UTMS(2.2 GHz), 4G-LTE(2.6 GHz) and 5G-IMT(3.6 GHz) are with the peak harvested power of around −9∼−10 dBm, which is equivalent to between 75% and 90% of the peak power at 2.4 GHz. At ISM-5.8 GHz, the peak power is greater than −9 dBm with beam alignment between the horn and the proposed antenna. In summary, it is proved that the demand of broadband wide-angle WEH and directional WPT could be realized simultaneously.

V. CONCLUSION

In this paper, a back-to-back microstrip antenna design for broadband wide-angle RF energy harvesting and dedicated wireless power transfer to address the issue of power supply for wireless sensor network. The 'ground mode' is introduced innovatively to form a broadband resonance from 2 GHz to 4 GHz to cover the mainstream communication bands and ISM bands. The broadband resonance is with omnidirectional radiation characteristics, which applies to harvest the energy of the incident waves of the communication bands. The design freedom brought by the loading of patches and shorting vias excites a resonance around 5.8 GHz, which is with bi-directional radiation characteristic and suitable for dedicated wireless power transfer. The measured results of antenna performance through multi-probe test platform and the WEH/WPT performance conform the results of full-wave simulation, which validate that the proposed antenna is expected to apply to power supply for wireless sensor network. The complete WEH and WPT system will also include rectification process to achieve RF-DC conversion. For broadband and multi-frequency WEH, high-efficient multi-frequency rectification will be another important task. How to integrate the two effectively will be the next research point.

REFERENCES

[1] L. Atzori, A. Iera, and G. Morabito, "The Internet of Things: A survey," *Comput. Netw.*, vol. 54, no. 15, pp. 2787–2805, Oct. 2010.
[2] X. Lu, P. Wang, D. Niyato, D. I. Kim, and Z. Han, "Wireless networks with RF energy harvesting: A contemporary survey," *IEEE Commun. Surveys Tuts.*, vol. 17, no. 2, pp. 757–789, 2nd Quart., 2015.
[3] S. Priya and D. J. Inman, *Energy Harvesting Technologies*. Boston, MA, USA: Springer, 2009.
[4] L. Li, H. Liu, H. Zhang, and W. Xue, "Efficient wireless power transfer system integrating with metasurface for biological applications," *IEEE Trans. Ind. Electron.*, vol. 65, no. 4, pp. 3230–3239, Apr. 2018.
[5] S. Yu, H. Liu, and L. Li, "Design of near-field focused metasurface for high-efficient wireless power transfer with multifocus characteristics," *IEEE Trans. Ind. Electron.*, vol. 66, no. 5, pp. 3393–4002, May 2019.
[6] C. R. Valenta and G. D. Durgin, "Harvesting wireless power: Survey of energy-harvester conversion efficiency in far-field, wireless power transfer systems," *IEEE Microw. Mag.*, vol. 15, no. 4, pp. 108–120, Jun. 2014.
[7] A. Khemar, A. Kacha, H. Takhedmit, and G. Abib, "Design and experiments of a dual-band rectenna for ambient RF energy harvesting in urban environments," *IET Microw., Antennas Propag.*, vol. 12, no. 1, pp. 49–55, Jan. 2018.
[8] L.-J. Xu, B. Huang, X. Bai, and H.-P. Mao, "A dualband and broadband antenna array for ambient RF energy harvesting," in *Proc. IEEE Int. Conf. Ubiquitous Wireless Broadband (ICUWB)*, Oct. 2016, pp. 1–3.
[9] D.-K. Ho, I. Kharrat, V.-D. Ngo, T.-P. Vuong, Q.-C. Nguyen, and M.-T. Le, "Dual-band rectenna for ambient RF energy harvesting at GSM 900 MHz and 1800 MHz," in *Proc. IEEE Int. Conf. Sustain. Energy Technol. (ICSET)*, Nov. 2016, pp. 306–310.
[10] S. Shen, C.-Y. Chiu, and R. D. Murch, "A dual-port triple-band L-probe microstrip patch rectenna for ambient RF energy harvesting," *IEEE Antennas Wireless Propag. Lett.*, vol. 16, pp. 3071–3074, 2017.
[11] C. Song, Y. Huang, P. Carter, J. Zhou, S. Yuan, Q. Xu, and M. Kod, "A novel six-band dual CP rectenna using improved impedance matching technique for ambient RF energy harvesting," *IEEE Trans. Antennas Propag.*, vol. 64, no. 7, pp. 3160–3171, Jul. 2016.
[12] C. Song, Y. Huang, J. Zhou, J. Zhang, S. Yuan, and P. Carter, "A high-efficiency broadband rectenna for ambient wireless energy harvesting," *IEEE Trans. Antennas Propag.*, vol. 63, no. 8, pp. 3486–3495, Aug. 2015.
[13] Y. Shi, Y. Fan, Y. Li, L. Yang, and M. Wang, "An efficient broadband slotted rectenna for wireless power transfer at LTE band," *IEEE Trans. Antennas Propag.*, vol. 67, no. 2, pp. 814–822, Feb. 2019.
[14] T. S. Almoneef, F. Erkmen, and O. M. Ramahi, "Harvesting the energy of multi-polarized electromagnetic waves," *Sci. Rep.*, vol. 7, no. 1, Nov. 2017, Art. no. 14656.
[15] L. Li, X. Zhang, C. Song, and Y. Huang, "Progress, challenges, and perspective on metasurfaces for ambient radio frequency energy harvesting," *Appl. Phys. Lett.*, vol. 116, no. 6, Feb. 2020, Art. no. 060501.
[16] B. Ghaderi, V. Nayyeri, M. Soleimani, and O. M. Ramahi, "Pixelated metasurface for dual-band and multi-polarization electromagnetic energy harvesting," *Sci. Rep.*, vol. 8, no. 1, Sep. 2018, Art. no. 13227.
[17] O. M. Ramahi, T. S. Almoneef, M. AlShareef, and M. S. Boybay, "Metamaterial particles for electromagnetic energy harvesting," *Appl. Phys. Lett.*, vol. 101, no. 17, Oct. 2012, Art. no. 173903.
[18] X. Zhang, H. Liu, and L. Li, "Electromagnetic power harvester using wide-angle and polarization-insensitive metasurfaces," *Appl. Sci.*, vol. 8, no. 4, p. 497, Mar. 2018.
[19] X. Zhang, H. Liu, and L. Li, "Tri-band miniaturized wide-angle and polarization-insensitive metasurface for ambient energy harvesting," *Appl. Phys. Lett.*, vol. 111, no. 7, Aug. 2017, Art. no. 071902.
[20] Y.-Y. Hu, S. Sun, H. Xu, and H. Sun, "Grid-array rectenna with wide angle coverage for effectively harvesting RF energy of low power density," *IEEE Trans. Microw. Theory Techn.*, vol. 67, no. 1, pp. 402–413, Jan. 2019.
[21] S. Shen, C.-Y. Chiu, and R. D. Murch, "Multiport pixel rectenna for ambient RF energy harvesting," *IEEE Trans. Antennas Propag.*, vol. 66, no. 2, pp. 644–656, Feb. 2018.
[22] M. Pinuela, P. D. Mitcheson, and S. Lucyszyn, "Ambient RF energy harvesting in urban and semi-urban environments," *IEEE Trans. Microw. Theory Techn.*, vol. 61, no. 7, pp. 2715–2726, Jul. 2013.
[23] S. Kim, R. Vyas, J. Bito, K. Niotaki, A. Collado, A. Georgiadis, and M. M. Tentzeris, "Ambient RF energy-harvesting technologies for self-sustainable standalone wireless sensor platforms," *Proc. IEEE*, vol. 102, no. 11, pp. 1649–1666, Nov. 2014.

[24] Y. K. Tan and S. K. Panda, "Energy harvesting from hybrid indoor ambient light and thermal energy sources for enhanced performance of wireless sensor nodes," *IEEE Trans. Ind. Electron.*, vol. 58, no. 9, pp. 4424–4435, Sep. 2011.
[25] J. Bito, R. Bahr, J. G. Hester, S. A. Nauroze, A. Georgiadis, and M. M. Tentzeris, "A novel solar and electromagnetic energy harvesting system with a 3-D printed package for energy efficient Internet-of-Things wireless sensors," *IEEE Trans. Microw. Theory Techn.*, vol. 65, no. 5, pp. 1831–1842, May 2017.
[26] K. Niotaki, A. Collado, A. Georgiadis, S. Kim, and M. M. Tentzeris, "Solar/electromagnetic energy harvesting and wireless power transmission," *Proc. IEEE*, vol. 102, no. 11, pp. 1712–1722, Nov. 2014.
[27] H. Yi, Y. Wang, and L. Li, "A novel broadband microstrip patch antenna with small ground plane," in *Proc. Cross Strait Quad-Regional Radio Sci. Wireless Technol. Conf. (CSQRWC)*, Jul. 2018, pp. 1–3.

PEI ZHANG was born in Yangzhou, China, in 1992. He received the B.E. degree in radio wave propagation and antenna from Xidian University, Xi'an, China, in 2017, where he is currently pursuing the Ph.D. degree in electromagnetic fields and microwave technology.

His research interests include wireless power transfer, wireless energy harvesting, metasurfaces, and electromagnetic field simulation and optimization.

HAO YI was born in Yueyang, China, in 1988. He received the B.E. and master's degrees in electromagnetic fields and microwave technology from Xidian University, Xi'an, China, in 2011 and 2014, respectively, where he is currently pursuing the Ph.D. degree in electromagnetic fields and microwave technology.

He joined a startup company focusing on millimeter wave radars as a Senior Antenna Engineer, in 2014. He has authored over ten Chinese patents. His research interests include millimeter wave antenna array, automotive radar antenna, and reflectarray and metasurface antenna.

HAIXIA LIU (Member, IEEE) was born in Hebei, China, in 1976. She received the B.S. and M.S. degrees in test and measurement technique and instrumentation and the Ph.D. degree in electromagnetic fields and microwave technology from Xidian University, Xi'an, China, in 1998, 2001, and 2014, respectively.

She studied at Shizuoka University, Shizuoka, Japan, as a Cooperative Graduate, in 2001. Since 2002, she has been working with Xidian University. Her research interests include circuit analysis, frequency measurement and control, wireless power transfer, antennas, and electromagnetic compatibility.

HONG YANG was born in Shanxi, China, in 1977. She received the B.Eng. and M.Eng. degrees from Central South University. She joined the First Research Institute of Ministry of Public Security of PRC as a Researcher, where she became a Full Researcher, in 2012.

GUOFEI ZHOU was born in Hunan, China. He received the B.E. degree in electrical engineering from Nanchang Hangkong University, Nanchang, China, in 1999, the M.S. degree in signal and information processing from Tianjin University, Tianjin, China, in 2003, and the Ph.D. degree in communication and information engineering from Tsinghua University, Beijing, China, in 2009.

He is currently an Associate Researcher with the First Research Institute of Ministry of Public Security of PRC, Beijing. His research interests include wireless power transfer, wireless energy harvesting, microwave communication, antennas, RF transceiver, RFIC design, and integrated circuit design for UHF RFID systems.

LONG LI (Senior Member, IEEE) received the B.E. and Ph.D. degrees in electromagnetic fields and microwave technology from Xidian University, Xi'an, China, in 1998 and 2005, respectively.

He was a Senior Research Associate with the Wireless Communications Research Center, City University of Hong Kong, in 2006. He received the Japan Society for Promotion of Science (JSPS) Postdoctoral Fellowship and visited Tohoku University, Sendai, Japan, as a JSPS Fellow, from 2006 to 2008. He was a Senior Visiting Scholar with Pennsylvania State University, USA, in 2014. He is currently a Professor with the School of Electronic Engineering, Xidian University. He is also the Director of the Key Laboratory of High Speed Circuit Design and EMC of Ministry of Education, and the Dean of the Hai-Tang No. 9 Academy, Xidian University. He has authored or coauthored over 100 articles in journals and held more than 20 patents. His research interests include metamaterials/metasurfaces, antennas and microwave devices, field-circuit collaborative design and EMC, wireless power transfer and harvesting technology, and OAM vortex waves.

Dr. Li is a Senior Member of CIE. He received the Nomination Award of National Excellent Doctoral Dissertation of China, in 2007; the Program for New Century Excellent Talents from the University of the Ministry of Education of China, in 2010; the IEEE APS Raj Mittra Travel Grant Senior Researcher Award, in 2015; the Shaanxi Youth Science and Technology Award, in 2016; and the Outstanding Young Foundation of Shaanxi Province of China. He won the Best Paper Award in the International Symposium on Antennas and Propagation, in 2008, and the First Prize of Awards for Scientific Research Results offered by the Shaanxi Provincial Department of Education, China, in 2013. He is the Vice President of the MTT-Chapter in the IEEE Xi'an Section. He is the TPC Co-Chair of APCAP2017 and the General Co-Chair of AWPT2019. He serves as an Associate Editor for the *Applied Computational Electromagnetics Society Journal* (ACES Journal) and a Guest Editor for the IEEE JOURNAL OF ELECTROMAGNETICS, RF AND MICROWAVES IN MEDICINE AND BIOLOGY (J-ERM) SPECIAL ISSUE.